Experimental and Molecular Pathology 109 (2019) 1–15

Contents lists available at ScienceDirect

Experimental and Molecular Pathology

journal homepage: www.elsevier.com/locate/yexmp

Immune profiling reveals the diverse nature of the immune response in NSCLC and reveals signaling pathways that may influence the anti-tumor immune response

Christopher A. Hamm*, Karen Pry, Jim Lu, Sarah Bacus

GoPath Laboratories, 1351 Barclay Blvd, Buffalo Grove, IL 60089, United States of America

ARTICLE INFO

Keywords:
Immunotherapy
CD8
PD-L1
IDO1
NSCLC

ABSTRACT

Recent FDA approvals of immunotherapy for NSCLC provide patients new treatment options, and these approvals also highlight the importance of the immune response in cancer treatment. While immunotherapy provides patients a new treatment option, the therapy is effective in less than half of the treated patients. To attain greater insight into the tumor-immune microenvironment, NSCLC tumors were analyzed by IHC and RNA-seq. IHC was used to identify NSCLC tumors that contain low, moderate, or high levels of CD8+ positive cells as a manifestation of an active anti-tumor immune response. Gene expression analysis identified an emergent gene signature that is associated with high and moderate levels of CD8 in NSCLC. In addition, the NSCLC tumors also express a unique combination of genes that may indicate complex anti-tumor immune responses (INFG-related genes, STATs, CXCL9, OX40, PD-L1, PD-L2, IDO1, and CD47). Several NSCLC tumors also express the immune checkpoint PD-L1 and at least one additional immune inhibitory molecule (IDO1, PD-L2, or others), which may explain the lack of a therapeutic response to treatments that disrupt only one immune checkpoint pathway.

1. Introduction

Lung cancer is one of the most common cancers worldwide. With over 1.8 million new cases of diagnosed each year, lung cancer accounts for > 1.6 million deaths a year (Dela Cruz et al., 2011; ACS, 2018). Approximately 85% of all lung cancers are classified as non-small cell lung cancer (NSCLC). The 5-year survival rate of advanced NSCLC cancer is < 20%, but recent advances in targeted therapy and immunotherapy have improved survival rates in subsets of NSCLC patients (Ettinger et al., 2017; J et al., 2017).

Recent advances in NSCLC immunotherapy are due to the use of immune checkpoint inhibitors, which target the immune inhibitory proteins programmed cell death protein 1 (PD-1) or programmed cell death protein ligand-1 (PD-L1). The FDA recently approved the PD-1 antibodies Pembrolizumab (Keytruda) and Nivolumab (Opdivo), and the PD-L1 antibody Atezolizumab (Tecentriq) for the treatment of NSCLC (Hematology, 2017). Although the PD-1 and PD-L1 antibodies provide an objective response in subsets of patients, only 15–30% of patients respond to individual immune checkpoint inhibitors and responders may ultimately develop therapeutic resistance (Malhotra et al., 2017; Somasundaram and Burns, 2017). While immunotherapy is effective in a subset of patients, other patients may experience treatment-related adverse events (Baxi et al., 2018), and a small percentage of patients may experience accelerated disease following treatment with an immune checkpoint inhibitor (Alomari et al., 2016; Champiat et al., 2017).

PD-L1 expression, as determined by immunohistochemistry, correlates with response to immune checkpoint inhibitors (Ramalingam et al., 2016). However, the use of PD-L1 as a standalone predictive biomarker is complicated by the observation that PD-L1 negative tumors may also respond to immune checkpoint inhibitors (Dang et al., 2016; Gettinger et al., 2016; Kang et al., 2017). Recent evidence indicates that tumor mutational burden (TMB) testing and Microsatellite instability (MSI) testing has predictive value in the identification of patients that may respond to immune checkpoint inhibitors (Kowanetz et al., n.d.; Chang et al., 2017). While current biomarker testing strategies provide selection criteria for the identification of patients that may respond to immune checkpoint therapies, additional biomarker research will improve patient stratification, minimize adverse events, and provide insight into biologic pathways that underlie a therapeutic response.

To attain a greater understating of immune signaling in NSCLC, RNA-seq and Immunohistochemistry (IHC) were used to profile the tumor-immune environment. The RNA and protein analysis provides

* Corresponding author at: GoPath Laboratories, 1351 Barclay Blvd, Buffalo Grove, IL 60089, United States of America
E-mail address: chamm@gopathlabs.com (C.A. Hamm).

https://doi.org/10.1016/j.yexmp.2019.04.004
Received 1 August 2018; Received in revised form 19 February 2019; Accepted 2 April 2019
Available online 03 April 2019
0014-4800/

A

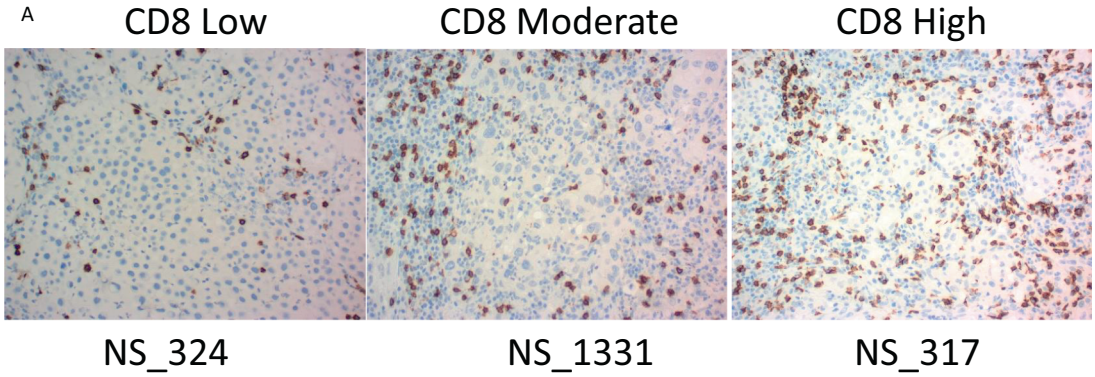

B

	Tissue	NS_323	NS_324	NS_325	NS_334	NS_336	NS_339	NS_349_n	NS_350_n	NS_351_n	NS_322	NS_342	NS_352	NS_1331	NS_1340	NS_1341	NS_1342	NS_317	NS_320	NS_326	NS_333	NS_343_n	NS_699_n
CD8 IHC	Tumor (TIL)	-	-	-	+	-	-	-	-	-	+	-	-	-	-	-	-	-	-	+	-	+	+
	Stroma	L	L	L	L	L	L	L	L	L	M	M	M	M	M	M	M	H	H	H	H	H	H
	Aggregates	+	-	-	-	-	+	-	-	-	+	+	-	+	+	+	+	-	-	+	+	+	-
	Area of CD8+ Regions (mm^2)	4.6	11.2	10.1	13.2	9.2	12.7	11.4	3.9	5.4	22.1	15.9	7.7	12.9	10.2	18.2	18.6	30.2	30.7	20.0	18.8	14.5	19.8

Fig. 1. NSCLC classified by the amount of CD8+ Positive cells. (A) CD8 IHC was used to characterize NSCLC tissues: low (Left panel), moderate (Center panel), or high (Right panel) levels of CD8+ cells (20×; scoring parameters are provided in Supplementary Table S1). (B) Summary of CD8 IHC in each NSCLC tissue. H: High, M: Moderate, and L: Low level of CD8+ cells. Pathologist IHC scoring parameters are provided in Supplementary Table S1. "Area of CD8+ Regions (mm^2)" refers to the total slide area of CD8+ regions (mm^2) as determined by microscope based image analysis.

insight into the immune microenvironment within each NSCLC tumor. The expression analysis also revealed that NSCLC tumors express unique combinations of genes related to the amount of CD8+ cells, immune activation, and immune inhibition, which may ultimately influence immune escape and response to immune checkpoint therapy.

2. Materials and methods

2.1. Immunohistochemistry

Formalin-fixed paraffin-embedded 5 µm sections were stained for CD3, CD8, CD163 FoxP3, PD1, PDL1, PDL2, phospho-STAT3, and IDO1 by immunohistochemistry. Antigen retrieval was performed on the Leica BondRx Autostainer utilizing Leica Epitope Retrieval solution 1 (Citrate) for IDO1, or Leica Epitope Retrieval Solution 2 (EDTA) for CD3, CD8, CD163, FoxP3, PD1, PDL1, PDL2, and phospho-STAT3. Staining was carried out on the Leica BondRx Autostainer. The sections were stained with a primary antibody to CD3 (Leica), CD8 (Leica) and CD163 (Leica) at a pre-dilute concentration for 15 min; phospho-Stat3 (Cell Signaling) at a 1: 100 dilution for 30 min; FoxP3 (Abcam), PD1 (Cell Signaling), PDL1 (Cell Signaling) and PDL2 (Cell Signaling) at a 1: 200 dilution for 30 min; and IDO1 (Cell Signaling). The Leica Bond Polymer Refine Detection System was utilized to complete the staining. Hematoxylin was used as the counterstain. The slides were scored and reviewed by two pathologists. The pathology scoring parameters are provided in Supplementary Table S1, and the Pathology scoring summary is provided in Supplementary Table S2. CD8 IHC Image analysis was performed with an Aeperio Scanscope XT using spectrum software (Algorithm: Positive Pixel Count v9) as previously described (Hamm et al., 2016).

2.2. NSCLC tissue and next-generation sequencing FFPE RNA

NSCLC tissue was obtained from Indivumed as tissue in FFPE blocks. All NSCLC FFPE tissues were histologically subtyped as adenocarcinoma of the lung, subtyping was performed by tissue morphology. Total RNA was isolated from FFPE samples with an Agencourt FormaPure Kit (protocol 000385v005) according to the manufacturer's protocol. RNA quantity was measured using a Nanodrop 8000, and the RNA quality was measured with the Agilent RNA 6000 Nano Kit. Approximately 400 ng of total RNA was used as input material for each RNA-seq assay. Each assay requires a minimum RNA quality of a DV200 > 50% (measurement of RNA integrity). All NSCLC tissue, discussed in this manuscript, had a DV200 score that was > 50%. Library construction and preliminary bioinformatics analyses was performed according to manufacturer's protocol (Qiagen: QIAseq Custom Targeted RNA Panel). Sequencing reactions were carried out on an Illumina MiSeq according to manufacturer's protocol (Illumina).

Briefly, the custom immune panel measures the expression of approximately 500 immune-related genes. NGS library metrics are presented in Supplementary Table S3, and the raw data is presented in Supplementary Table S3. Each RNA-seq library was normalized to 1×10^6 molecular tags (Table S4). The RNA panel also contains control probes to measure any potential genomic DNA contamination. None of the FFPE samples contained detectible levels of genomic DNA. RNA-seq data was analyzed for differential expression using a Student's *t*-test ($p < .05$; "CD8 Low tissues vs CD8 Moderate Tissues" and "CD8 Low tissues vs CD8 High Tissues"). The *p*-values were calculated based on a Student's *t*-test of the normalized gene expression values for each gene in a given comparison (ex. "CD8 Low tissues vs CD8 Moderate Tissues" or "CD8 Low tissues vs CD8 High Tissues").

2.3. Heat maps, hierarchical clustering, and pathway mapping

Heat maps were created with normalized RNA-seq data using Morpheus Software (Broad Institute; https://software.broadinstitute.org/morpheus/). Each Heat Map uses a relative color scheme for each row (A relative color scheme uses the minimum and maximum values in

Table 1
Genes differentially expressed between CD8 Low NSCLC tissues and CD8 moderate NSCLC tissues (Normalized Data).

Normalized RNA-Seq data: "CD8 Low" tissues vs CD8 "Moderate" Tissues ($p < .05$)									
Gene Symbol	CD8 Low								
	NS_323_n	NS_324_n	NS_325_n	NS_334_n	NS_336_n	NS_339_n	N_S350_n	NS_349_n	NS_351_n
BTK	79	179	449	248	177	243	108	289	193
BTLA	13	35	46	40	35	28	11	88	41
C3AR1	98	75	325	301	226	272	139	296	424
CCL19	55	183	362	244	238	136	150	241	416
CCL5	1036	3420	3858	2490	3511	1352	1661	4204	2265
CCR2	32	88	68	134	80	107	40	137	82
CCR5	29	64	87	206	95	94	79	119	167
CCR7	12	31	129	86	96	44	22	57	65
CD2	61	183	197	262	192	140	55	255	136
CD3D	214	669	829	565	1114	519	329	1374	669
CD3E	93	146	442	346	457	221	181	523	419
CD3G	6	31	31	59	39	33	8	48	51
CD4	221	636	1155	1020	853	1120	690	778	1182
CD5	18	75	82	80	89	54	32	61	43
CD7	275	289	271	328	253	108	62	159	146
CD70	25	13	24	10	21	13	6	16	25
CD8A	50	148	340	294	175	86	98	178	101
CD8B	12	108	60	62	32	29	18	34	33
CLEC4E	12	60	99	170	159	70	79	173	306
CTLA4	16	55	40	60	63	56	11	49	54
CXCL11	66	33	63	313	53	32	36	73	64
CXCL13	102	104	1227	709	406	28	477	364	326
CXCL9	185	207	822	1525	1019	115	502	851	987
CXCR3	15	31	36	70	72	22	18	30	34
CXCR5	–	–	23	10	7	3	–	3	10
CXCR6	14	55	57	97	39	20	28	48	36
EOMES	12	42	61	114	60	23	54	64	28
FASLG	8	66	25	40	21	11	12	24	13
FGL2	132	278	396	670	230	331	241	478	581
FLT3	5	9	21	22	9	11	6	26	13
FLT3LG	64	161	190	217	164	120	138	126	164
GFI1	30	124	108	146	104	36	78	98	61
GZMA	62	196	176	447	225	96	92	224	118
ICOS	15	29	152	87	112	75	32	78	113
IL10RA	107	505	601	384	382	218	287	405	337
IL12B	1	2	2	–	1	2	–	3	2
IL12RB1	20	126	61	102	51	26	37	49	54
IL16	139	424	762	336	464	367	213	517	535
IL21R	23	55	52	72	36	48	29	40	70
IL2RB	50	159	181	244	181	100	86	119	151
IL7R	139	166	961	460	747	398	126	498	293

(*continued on next page*)

Table 1 (*continued*)

Normalized RNA-Seq data: "CD8 Low" tissues vs CD8 "Moderate" Tissues ($p < .05$)									
Gene Symbol	CD8 Low								
	NS_323_n	NS_324_n	NS_325_n	NS_334_n	NS_336_n	NS_339_n	N_S350_n	NS_349_n	NS_351_n
INHBA	309	40	733	798	683	1023	592	437	1013
IRF4	24	113	121	64	109	49	46	256	72
JAK3	119	177	221	180	237	144	168	147	133
LCK	11	55	63	36	69	34	14	80	75
LGALS3	2682	3365	3638	3338	2984	7858	7132	4365	5259
NR3C1	316	554	667	595	366	457	532	622	676
POU2F2	29	159	149	99	169	50	137	163	136
PTPRC	13	4	43	31	24	23	18	23	21
SELL	49	90	342	193	218	146	150	142	157
TLR6	14	26	44	40	27	16	16	29	39
TLR9	2	13	19	19	33	6	12	20	15
TNFSF8	20	68	76	43	49	38	32	49	49
TP53INP1	211	472	1241	579	617	303	416	1014	545
VAV1	113	386	432	339	324	207	150	255	267
VCAM1	257	66	840	392	582	579	414	265	417

Normalized RNA-Seq data: "CD8 Low" tissues vs CD8 "Moderate" Tissues ($p < .05$)									
Gene Symbol	CD8 Low	CD8 Moderate							
	NS_323_n	NS_1340_n	Ns_1341_n	NS1342_n	NS_322_n	NS_342_n	NS_352_n	Average Expression in CD8 Moderate Tissues	Fold change
BTK	79	449	321	493	357	445	139	363	1.67
BTLA	13	154	45	94	99	71	17	77	2.06
C3AR1	98	607	539	540	581	176	290	444	1.85
CCL19	55	632	215	1124	731	372	231	567	2.52
CCL5	1036	4336	13,671	3847	7452	2936	3600	5721	2.16
CCR2	32	313	231	207	186	162	66	192	2.25
CCR5	29	228	205	198	242	98	104	178	1.70
CCR7	12	275	88	124	190	98	42	136	2.26
CD2	61	468	343	395	623	388	156	372	2.26
CD3D	214	1156	858	1250	2289	1137	778	1259	1.80
CD3E	93	918	577	537	1296	329	417	681	2.17
CD3G	6	80	82	94	114	63	31	76	2.23
CD4	221	1306	1223	1583	1829	974	629	1242	1.46
CD5	18	125	111	195	170	79	49	126	2.12
CD7	275	393	249	513	682	375	294	405	1.93
CD70	25	48	35	27	26	51	14	34	2.01
CD8A	50	542	538	421	865	196	153	415	2.54
CD8B	12	90	82	83	110	228	47	97	2.26
CLEC4E	12	534	154	273	200	136	289	322	2.57
CTLA4	16	106	92	130	140	93	29	95	2.11

(*continued on next page*)

Table 1 (*continued*)

Normalized RNA-Seq data: "CD8 Low" tissues vs CD8 "Moderate" Tissues ($p < .05$)

Gene Symbol	CD8 Low	CD8 Moderate							
	NS_323_n	NS_1340_n	Ns_1341_n	NS1342_n	NS_322_n	NS_342_n	NS_352_n	Average Expression in CD8 Moderate Tissues	Fold change
CXCL11	66	166	223	413	300	86	147	205	2.51
CXCL13	102	1422	397	1778	1922	836	336	1050	2.53
CXCL9	185	1249	594	4669	6682	778	2309	2514	3.64
CXCR3	15	80	76	103	110	70	27	77	2.10
CXCR5	–	18	9	26	25	10	5	15	2.40
CXCR6	14	107	63	94	149	51	33	82	1.88
EOMES	12	174	236	109	217	76	52	130	2.56
FASLG	8	37	53	62	88	49	24	48	1.96
FGL2	132	773	671	860	1142	369	328	667	1.80
FLT3	5	80	28	35	38	19	3	32	2.35
FLT3LG	64	255	208	257	284	374	139	240	1.61
GFI1	30	207	172	137	254	268	65	191	2.20
GZMA	62	358	272	455	726	249	200	349	1.92
ICOS	15	159	151	151	310	120	52	159	2.06
IL10RA	107	564	595	695	594	798	347	612	1.71
IL12B	1	3	3	2	5	5	–	3	2.24
IL12RB1	20	101	107	145	119	100	51	109	1.86
IL16	139	1044	642	874	946	1422	228	854	2.05
IL21R	23	58	138	218	169	130	34	126	2.68
IL2RB	50	336	226	351	489	315	150	309	2.19
IL7R	139	1841	976	635	726	900	353	871	2.07
INHBA	309	712	1165	1162	1014	1310	344	1049	1.68
IRF4	24	168	288	303	288	741	79	332	3.51
JAK3	119	244	231	290	303	253	193	255	1.51
LCK	11	116	72	112	113	76	42	88	1.81
LGALS3	2682	4303	1648	1982	2611	3897	2984	2662	0.59
NR3C1	316	508	440	388	383	448	264	398	0.75
POU2F2	29	261	346	225	352	336	125	297	2.45
PTPRC	13	52	32	44	56	40	15	39	1.76
SELL	49	674	288	219	378	223	85	363	2.19
TLR6	14	78	52	33	37	59	16	49	1.76
TLR9	2	30	22	21	25	36	15	27	1.78
TNFSF8	20	222	84	85	124	97	32	113	2.38
TP53INP1	211	656	909	1164	695	1644	930	1091	1.82
VAV1	113	703	444	579	561	649	207	516	1.88
VCAM1	257	393	906	857	962	1139	447	758	1.79

Table 2
Genes differentially expressed between CD8 Low NSCLC tissues and CD8 High NSCLC tissues (Normalized Data).

Normalized RNA-Seq data: "CD8 Abuntant" tissues vs CD8 Low" Tissues ($p < .05$)

Gene symbol	CD8 Low NSCLC Tissue										CD8 High NSCLC Tissue							
	NS_323_n	NS_324_n	NS_325_n	NS_334_n	NS_336_n	NS_339_n	NS_350_n	NS_349_n	NS_351_n	Average Expression in CD8 Low Tissues	NS_317_n	NS_320_n	NS_326_n	NS_333_n	NS_343_n	NS_699_n	Average Expression in CD8 Abundant Tissues	Fold hange
BMP4	214	229	421	402	264	909	789	481	1363	564	64	139	301	274	108	313	200	0.35
CCL4	1459	2094	3745	2244	2168	1253	1312	5823	1931	2448	3894	5807	2754	1884	6635	5586	4427	1.81
CCL5	1036	3420	3858	2490	3511	1352	1661	4204	2265	2644	11,502	9418	8501	5581	6693	7155	8142	3.08
CCR5	29	64	87	206	95	94	79	119	167	104	199	291	267	280	125	154	219	2.10
CCR7	12	31	129	86	96	44	22	57	65	60	110	117	179	456	73	142	180	2.99
CD2	61	183	197	262	192	140	55	255	136	165	426	504	583	676	227	227	441	2.68
CD3D	214	669	829	565	1114	519	329	1374	669	698	1880	1730	1757	1323	1348	1802	1640	2.35
CD3E	93	146	442	346	457	221	181	523	419	314	968	808	810	963	548	903	833	2.65
CD3G	6	31	31	59	39	33	8	48	51	34	108	139	116	149	37	82	105	3.09
CD4	221	636	1155	1020	853	1120	690	778	1182	850	1087	1649	1422	1636	590	1156	1257	1.48
CD5	18	75	82	80	89	54	32	61	43	59	101	169	247	194	27	85	137	2.31
CD7	275	289	271	328	253	108	62	159	146	210	599	989	450	872	286	280	579	2.76
CD70	25	13	24	10	21	13	6	16	25	17	23	107	144	108	182	15	96	5.65
CD86	240	430	821	786	767	627	379	614	663	592	913	1556	869	981	545	843	951	1.61
CD8A	50	148	340	294	175	86	98	178	101	163	1209	1451	865	673	418	334	825	5.05
CD8B	12	108	60	62	32	29	18	34	33	43	142	292	149	201	72	57	152	3.54
CLEC4E	12	60	99	170	159	70	79	173	306	125	455	287	410	438	178	347	352	2.81
CMKLR1	39	181	203	236	139	111	103	140	196	150	220	455	246	329	125	173	258	1.72
CRTAM	10	35	100	40	55	60	32	63	59	50	86	86	74	116	55	65	80	1.59
CTLA4	16	55	40	60	63	56	11	49	54	45	67	118	134	168	37	64	98	2.19
CXCL10	144	181	186	1403	246	104	188	179	308	326	1261	831	2955	580	2355	201	1364	4.18
CXCL13	102	104	1227	709	406	28	477	364	326	416	2017	1637	6017	4779	338	3586	3062	7.36
CXCL9	185	207	822	1525	1019	115	502	851	987	690	4343	1920	3888	2429	2161	891	2605	3.77
CXCR3	15	31	36	70	72	22	18	30	34	36	81	145	95	130	22	40	86	2.35
CXCR5	–	–	23	10	7	3	–	3	10	6	16	10	31	60	8	29	26	4.09
CXCR6	14	55	57	97	39	20	28	48	36	44	97	151	106	121	42	61	96	2.21
EIF2AK2	2104	2213	668	1407	1343	1064	1719	770	1313	1400	580	1082	754	1050	1011	646	854	0.61
EOMES	12	42	61	114	60	23	54	64	28	51	87	130	242	266	99	101	154	3.03
FASLG	8	66	25	40	21	11	12	24	13	24	142	142	74	54	42	21	79	3.25
FGL2	132	278	396	670	230	331	241	478	581	371	577	908	777	724	477	411	646	1.74
GBP1	1106	1209	1590	4858	991	665	532	613	1439	1445	5170	3565	3427	2097	7790	1581	3938	2.73
GFI1	30	124	108	146	104	36	78	98	61	87	183	337	166	328	73	115	200	2.30
GZMA	62	196	176	447	225	96	92	224	118	182	657	1432	521	502	657	279	675	3.71
GZMH	131	1441	402	528	621	210	225	594	280	492	1795	1843	1483	753	1344	737	1326	2.69
ICOS	15	29	152	87	112	75	32	78	113	77	120	183	245	243	94	158	174	2.26
IFNG	1	18	9	32	8	2	11	8	7	11	94	67	44	20	51	20	49	4.69
IL10	11	40	34	32	25	20	26	45	36	30	26	96	34	64	37	67	54	1.81
IL12RB1	20	126	61	102	51	26	37	49	54	58	109	179	86	131	55	75	106	1.81
IL18	303	666	369	436	172	445	117	406	584	389	674	588	520	1219	599	339	656	1.69
IL18RAP	9	35	68	62	29	10	7	44	28	33	86	136	48	55	37	45	68	2.08
IL21	–	–	2	7	7	2	–	1	2	2	3	7	7	4	6	8	6	2.57
IL21R	23	55	52	72	36	48	29	40	70	47	96	95	175	177	47	76	111	2.35
IL2RA	61	282	226	398	488	156	172	166	257	245	302	586	1144	583	186	427	538	2.20
IL2RB	50	159	181	244	181	100	86	119	151	141	483	557	522	435	227	194	403	2.85
IL2RG	120	803	605	381	498	307	218	632	394	440	866	743	922	924	286	551	715	1.63
JAK2	116	274	305	472	211	179	176	327	260	258	336	346	681	562	665	220	468	1.82
JAK3	119	177	221	180	237	144	168	147	133	169	233	249	389	344	110	251	263	1.55

(*continued on next page*)

Table 2 (*continued*)

Normalized RNA-Seq data: "CD8 Abuntant" tissues vs CD8 Low" Tissues ($p < .05$)																			
Gene symbol	CD8 Low NSCLC Tissue										Average Expression in CD8 Low Tissues	CD8 High NSCLC Tissue							Average Expression in CD8 Abundant Tissues	Fold hange
	NS_323_n	NS_324_n	NS_325_n	NS_334_n	NS_336_n	NS_339_n	NS_350_n	NS_349_n	NS_351_n			NS_317_n	NS_320_n	NS_326_n	NS_333_n	NS_343_n	NS_699_n		
LCK	11	55	63	36	69	34	14	80	75		49	78	92	57	115	41	109	82	1.69
LGALS3	2682	3365	3638	3338	2984	7858	7132	4365	5259		4513	1654	3892	1210	4341	1892	2519	2585	0.57
PDCD1	10	82	29	29	24	11	17	15	20		26	65	100	50	63	19	73	62	2.34
POU2F2	29	159	149	99	169	50	137	163	136		121	256	142	187	720	191	347	307	2.54
PRF1	44	335	321	478	209	264	78	231	77		226	893	2303	498	444	462	246	808	3.57
PTPRC	13	4	43	31	24	23	18	23	21		22	32	62	66	85	11	42	50	2.25
RUNX1	2237	2979	2313	3119	3985	4117	3933	1774	4051		3168	1500	2052	2183	2884	2918	1817	2226	0.70
SH2D1A	–	–	1	1	–	–	–	1	2		0	3	3	6	2	2	1	3	5.66
TBX21	10	84	55	52	33	19	19	54	25		39	94	111	71	91	53	53	79	2.02
TNFRSF9	40	84	63	85	188	83	35	59	93		81	209	186	454	144	88	87	195	2.40
TNFSF8	20	68	76	43	49	38	32	49	49		47	67	181	70	179	20	114	105	2.22

each row to convert values to colors). Where noted, hierarchical clustering was used to sort the tissue (columns) and genes (rows) as described in heat maps. Hierarchical clustering (one minus the Pearson correlation) was performed using Morpheus Software (Broad Institute; broadinstitute.org/morpheus/). Pathway mapping was performed using Gene set enrichment analysis (GSEA) Broad Institute: http://software.broadinstitute.org/gsea/ (Subramanian et al., 2005).

3. Results

3.1. CD8+ levels in NSCLC

Tumor infiltrating lymphocytes (TILs) are a component of tumor the microenvironment in NSCLC (Trojan et al., 2004). The TIL levels, subtype, and activation status may influence clinical outcome (Fridman et al., 2012), and CD8 cell infiltrate density provides information on disease prognosis and responsiveness to immunotherapy (Galon et al., 2013). Therefore, IHC was used to classify the amount of CD8+ T-cells in the NSCLC tissues. The amount of CD8+ T-cells varied among NSCLCs, and NSCLCs were classified as having low, moderate, or high levels of CD8+ T-cells (Fig. 1). Of the 22 NSCLC tissues, 9 tissues contained low levels of CD8+ T-cells, 7 tissues contained moderate levels of CD8+ T-cells, and 6 tissues contained high levels of CD8+ T-cells. CD8+ T-cells presented as single cell spreads or as aggregates. CD8+ T-cells aggregate were observed more frequently in the tissues with moderate and high levels of CD8+ T-cells (Fig. 1B). Additional, pathology was confirmed using microscope based image analysis (Fig. 1B).

3.2. Immune gene expression in NSCLC

CD8 cell levels in the NSCLC tissue may be related to the signaling pathways that regulate the immune response in each tissue. Therefore, a targeted RNA-seq panel was used to profile the expression of genes that may regulate immune cells in NSCLC. The targeted RNA-seq panel consisted of 500 immune related genes. The RNA-seq analysis was performed on 22 NSCLC tissues. The RNA-seq library metrics and the complete RNA-seq (raw data and normalized) expression values are located in Supplementary Table S3 and S4.

The RNA-seq data was separated into one of three groups based on the level of CD8+ cells in the specific tissue and classified as containing low, moderate, or high levels of CD8+ cells (determined by IHC; Fig. 1). The RNA-seq data revealed gene expression changes between the NSCLC tissues with low, moderate, or high levels of CD8+ cells. Fifty-six genes are significantly differentially expressed between CD8 low NSCLC tissues and CD8 moderate NSCLC tissues (Table 1). In addition, 58 genes are significantly differentially expressed between CD8-low NSCLC tissues and CD8-high NSCLC tissues (Table 2).

Hierarchical clustering of the differentially expressed genes reveals that NSCLC samples cluster into two overall groups (Fig. 2). CD8-high tissues cluster into one group and CD8-low tissues cluster in another group (Fig. 2). However, CD8-moderate samples cluster among CD8-high samples (4 CD8-moderate tissues, see Fig. 2) and CD8-low tissues (3 CD8-moderate tissues, see Fig. 2). Despite the limited number of NSCLC samples, the clustering reveals a putative gene expression signature that may correlate with tissues that are classified as CD8-high and CD8-low. The clustering analysis also reveals that certain CD8-moderate tissues (classified by CD8 IHC) possess immune gene expression signatures that share a resemblance to expression the profiles of CD8-low tissues or CD8-high tissues. Although classified as CD8-moderate (classified by IHC), the heterogeneity of the CD8-moderate tissues may reflect an immune landscape that lies in-between the CD8-Low and CD8 high tissues, which highlights the importance of combining CD8 IHC with gene expression profiling to attain greater insight into pathways that contribute to the immune response in NSCLC.

Subsequent, pathway analysis revealed that the differentially

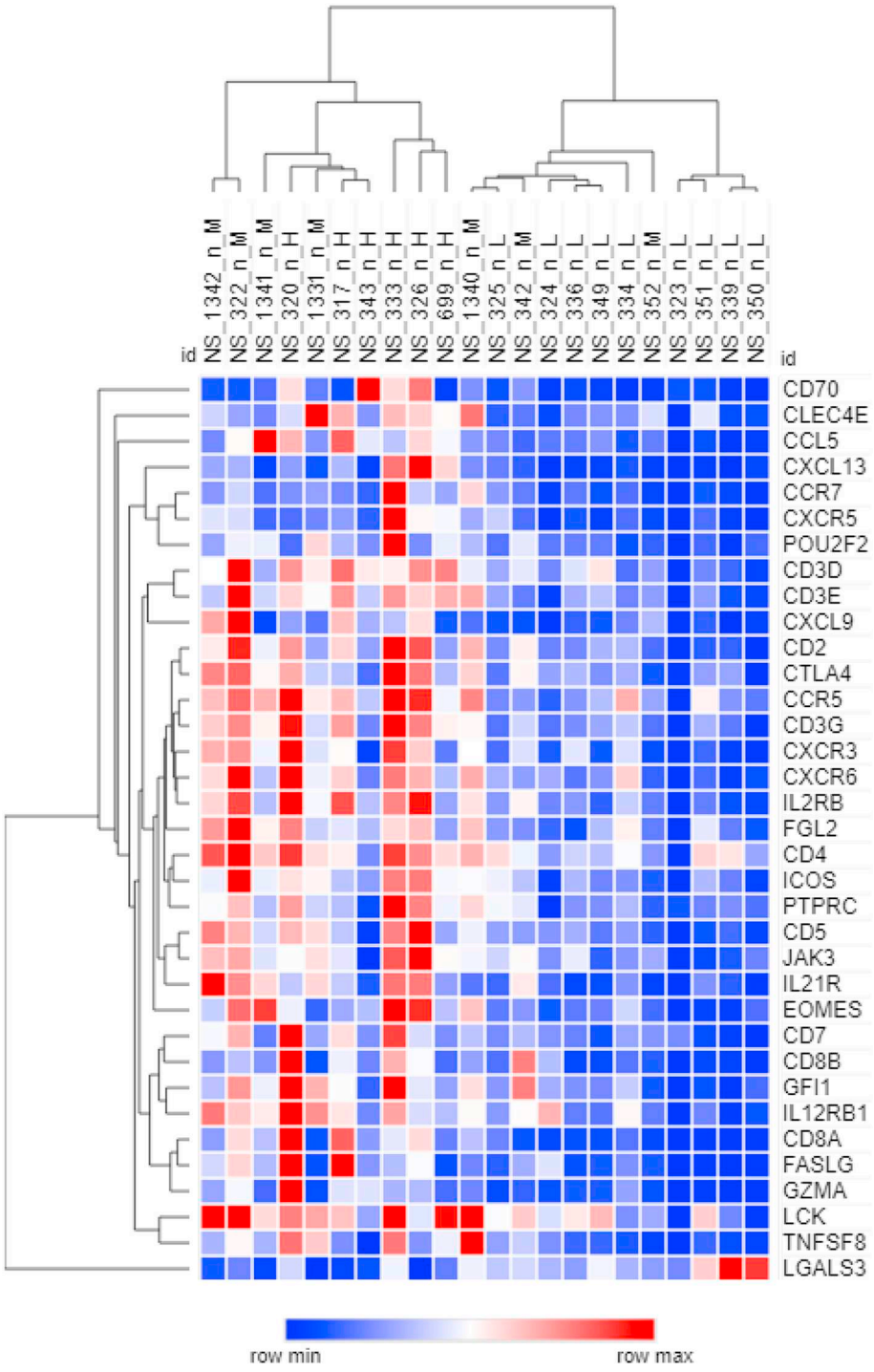

Fig. 2. Hierarchical Clustering of genes differentially expressed between NSCLC tissues characterized by Low, Moderate (Table 1), and High (Table 2) levels of CD8+ cells. To be included in this heat map, each gene must be listed in both Table 1 (CD8 low vs CD8 moderate) and Table 2 (CD8 Low vs CD8 high tissue). Hierarchical clustering reveals that CD8 low samples tend to cluster closely together, whereas CD8 high samples tend to cluster closely together. Notice the emergence of a potential gene signature associated with CD8+ levels in NSCLC tissues. On the vertical axis, note that tissue names are following by a "_n_" which indicates that normalized data was used for the heat map. The tissue name also includes either an H, M, or L (H: High, M: Moderate, and L: Low), which indicates the level of CD8 cells as determined in Fig. 1.

Table 3
Pathway Analysis of Differentially Expressed Genes (CD8 Low vs CD8 Moderate Tissue) (Normalized Data).

Pathway Analysis of Differentially Expressed Genes (CD8 Low vs CD8 Moderate Tissue)				
Gene Set Name [# Genes (K)]	Description	# Genes in Overlap (k)	p-value	FDR q-value
ALLOGRAFT_REJECTION	Genes up-regulated during transplant rejection.	26	4.43 e−47	1.06 e−44
INFLAMMATORY_RESPONSE	Genes defining inflammatory response.	14	2.72 e−21	3.25 e−19
IL2_STAT5_SIGNALING	Genes up-regulated by STAT5 in response to IL2 stimulation.	9	2.97 e−12	1.77 e−10
INTERFERON_GAMMA_RESPONSE	Genes up-regulated in response to IFNG.	9	2.97 e−12	1.77 e−10
IL6_JAK_STAT3_SIGNALING	Genes up-regulated by IL6 via STAT3.	4	4.08 e−6	1.62 e−4

Table 4
Pathway Analysis of Differentially Expressed Genes (CD8 Low vs CD8 High Tissue) (Normalized Data).

Pathway Analysis of Differentially Expressed Genes (CD8 Low vs CD8 High Tissue)				
Gene Set Name [# Genes (K)]	Description	# Genes in Overlap (k)	p-value	FDR q-value
ALLOGRAFT_REJECTION	Genes up-regulated during transplant rejection.	30	3.89 e−56	9.29 e−54
INFLAMMATORY_RESPONSE	Genes defining inflammatory response.	14	4.72 e−21	5.64 e−19
IL2_STAT5_SIGNALING	Genes up-regulated by STAT5 in response to IL2 stimulation.	10	8.45 e−14	5.05 e−12
INTERFERON_GAMMA_RESPONSE	Genes up-regulated in response to IFNG.	10	8.45 e−14	5.05 e−12
IL6_JAK_STAT3_SIGNALING	Genes up-regulated by IL6 via STAT3.	6	1.44 e−9	6.91 e−8

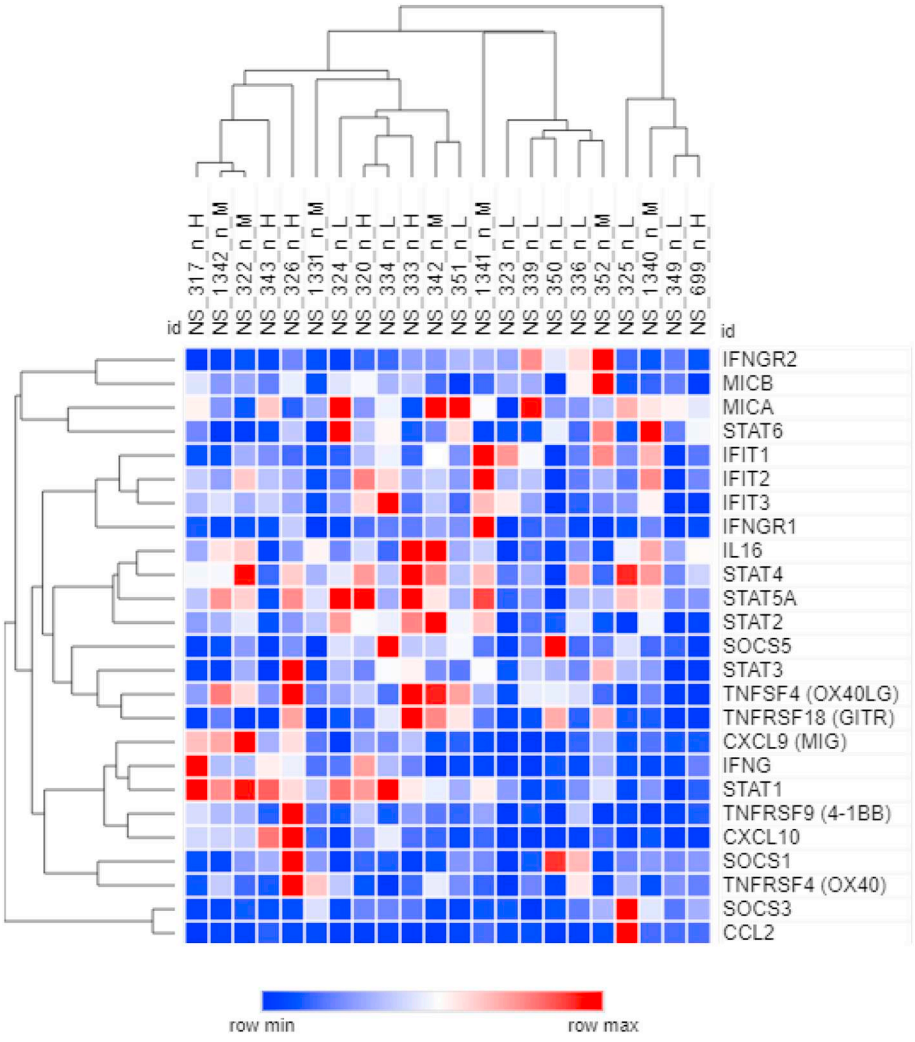

Fig. 3. Heat map of genes associated with immune activation (RNA-seq Data). For visualization, Heat Map uses a relative color scheme for each row. The relative color scheme uses the minimum and maximum values in each row to convert expression values to colors. Figure contains a subset of genes that were identified from the literature as having a putative role in immune cell activation. The normalized expression values were clustered using hierarchical clustering (one minus the Pearson correlation). The normalized expression values are listed in Supplementary Table S8. On the vertical axis, note that tissue names are following by a "_n_" which indicates that normalized data was used for the heat map. The tissue name also includes either an H, M, or L (H: High, M: Moderate, and L: Low), which indicates the level of CD8 cells as determined in Fig. 1.

expressed genes function in immune relevant pathways such as "Allograft Rejection" and "Interferon Gamma Response" (Tables 3 and 4). It is noteworthy that the CD8-high and CD8-moderate tissues express similar gene expression pathways. However, the CD8 -high tissues have a greater representation in each pathway (See Supplementary Table S6 and S7 for the specific list of genes that contribute to each pathway map).

Not surprisingly, the CD8-high and CD8-moderate tissues express elevated levels of T cell-related genes (ex. CD8A, GZMA, GZMH, etc.) and chemokines (ex. CXCL9 (MIG), CXCL10, etc.), which may be a component of active immune response in the NSCLC tissues (Tables 1 and 2) (Oelkrug and Ramage, 2014). Although CD8+ tissues express genes that may be relevant to an active immune environment, it is noteworthy that the same tissues also express inhibitory molecules that may disrupt the anti-tumor immune response. For example, CTLA4, PDCD1 (PD-1), and TBX21 (T-bet) are expressed at higher levels in the CD8 high tissue than CD8 low tissues (Table 2).

3.3. Expression of genes that regulate immune activation and immune suppression

Although the putative CD8 gene signature data provide insight into the genes that are associated the presence of CD8 (CD8 low, moderate, and high) tissues, NSCLCs are known as heterogeneous tumors (Chen et al., 2014). Therefore, the RNA-seq data was used to specifically examine immune-related genes in each NSCLC tissue (immune activation genes: Fig. 3; and immune inhibition genes: Fig. 4) (De Simone et al., 2016; Pardoll, 2012; Benci et al., 2016). The RNA-seq analysis revealed heterogeneity with respect to genes that play a role in the activation or the inhibition of an anti-tumor immune response (Figs. 3 and 4) (De

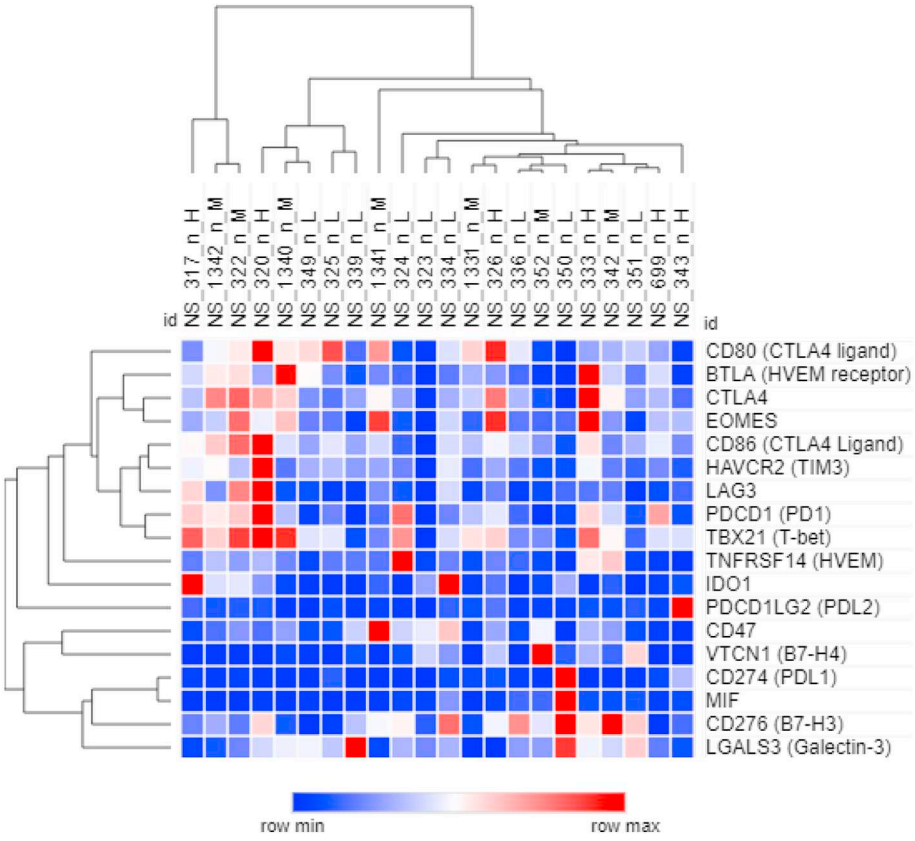

Fig. 4. Heat map of genes associated with immune inhibition (RNA-seq Data). For visualization, Heat Map uses a relative color scheme for each row. The relative color scheme uses the minimum and maximum values in each row to convert expression values to colors. Figure contains a subset of genes that were selected from the literature as having a putative role in inhibiting the immune response. The normalized expression values were clustered using hierarchical clustering (one minus the Pearson correlation). The normalized expression values are listed in Supplementary Table S9. On the vertical axis, note that tissue names are following by a "_n_" which indicates that normalized data was used for the heat map. The tissue name also includes either an H, M, or L (H: High, M: Moderate, and L: Low), which indicates the level of CD8 cells as determined in Fig. 1.

Simone et al., 2016; Pardoll, 2012; Benci et al., 2016). Several tissues express immune activation-related genes (ex. STAT pathway and chemokines; Fig. 3), whereas several tissues also express immune inhibitory molecules (Fig. 4).

For example, tissues NS_320, NS_326, and NS_333 express multiple genes related to both immune activation signaling and immune inhibitory signaling (Figs. 3 and 4), and these samples are also characterized by high levels of CD8 cells (Fig. 1B). Alternatively, tissue NS_351 expresses low levels of immune activation signaling and immune inhibitory signaling (Figs. 3 and 4; NS_351), which correlates with the IHC observation that tissue NS_351 contains a low level of CD8 cells.

Additionally tissues NS_343 and NS_350 both express genes associated with immune activation (Fig. 3). However, tissue NS_343 expresses the inhibitory molecules PD-L1, PD-L2 (PDCD1LG2), and IDO1 (Fig. 4). Whereas NS_350 expresses high levels of CD274 (PD-L1), IDO1, MIF, CD276 (B7-H3), and LGALS3 (Galectin-3) (Fig. 4) (Kouo et al., 2015).

The expression of the immune checkpoint molecule PD-L1 varies among NSCLC tissues, with highest levels of PD-L1 detected in samples NS_350, NS_343, NS_325, and NS_326. The expression of IDO1 (a gene that may promote immune tolerance to tumor antigens (Munn and Mellor, 2007)) also varied among tumor tissues. Tissues NS_317 and NS_334 expressed the highest levels of IDO1, whereas tissues NS_336 and NS_351 express low levels of IDO1. Additionally, CD47, an inhibitor of macrophage phagocytosis (Liu et al., 2017), is expressed at lower levels throughout most tissues, but CD47 expression is elevated in NS_1341 and NS_334. LAG3, a negative regulator of T cell activation is expressed at the highest levels in NS_320, _NS_322, and NS_317 (Workman et al., 2004; Workman and Vignali, 2003). The T-cell exhaustion markers T-bet (TBX21) and EOMES are also expressed in several tissues, albeit at low levels. The expression of T-bet and EOMES may indicate the presence of exhausted T-cells, which may have limited ability to respond to an immune checkpoint inhibitor (Wherry and Kurachi, 2015).

Finally, while the NSCLC RNA-seq data reveals some heterogeneity among immune activation and immune inhibitory genes, it is noteworthy that the hierarchical clustering reveals subsets of NSCLC that express similar combinations of genes (Figs. 3 and 4). For example, tissues NS_317, NS_1342, and NS_322 cluster together in heat maps (Figs. 3 and 4) and these tissues simultaneously express genes that function in immune activation and immune inhibition.

3.4. IHC confirms the simultaneous expression of multiple immune inhibitory proteins

The RNA-seq data provides insight into the genes and pathways that are expressed in NSCLC, but it is also important to determine if the immune pathways are also active on the protein level. In addition to the CD8 analysis (Fig. 1), IHC was used to measure the expression of the following immune-related genes: CD3, CD163, pSTAT3 (phosphorylated STAT3), FOXOP3, PD1, PD-L1 (CD274), PDL2 (PDCD1), and IDO1. The summary of the IHC data is presented in Supplementary Table S2, and the scoring parameters are listed in Table S1. Of the genes with both RNA-seq data and IHC data, all NSCLC samples with protein expression by IHC were also shown to express the corresponding RNA (Supplementary Table S2). Genes with moderate to high expression by RNA-seq correlated with the protein levels identified by IHC (CD8, PD-L1, PD-L2, and IDO1). PD-1 and FOXP3 were also detected by both RNA-seq and IHC, but direct correlation with protein expression should be carefully considered as these genes are expressed at relatively low levels in the RNA-seq data. In the RNA-seq data, PD-1 and Foxp3 genes are expressed at < 100 transcript counts in a given tissue.

Overall, the level of protein expression varies by tissue and IHC target, however, the most abundantly expressed genes, assessed by RNA-seq, are also expressed at high levels in the IHC analysis. PD-L1 RNA is expressed at highest levels in tissues NS_343 and NS_350, and the IHC confirms that both tissues express high levels of PD-L1 in the

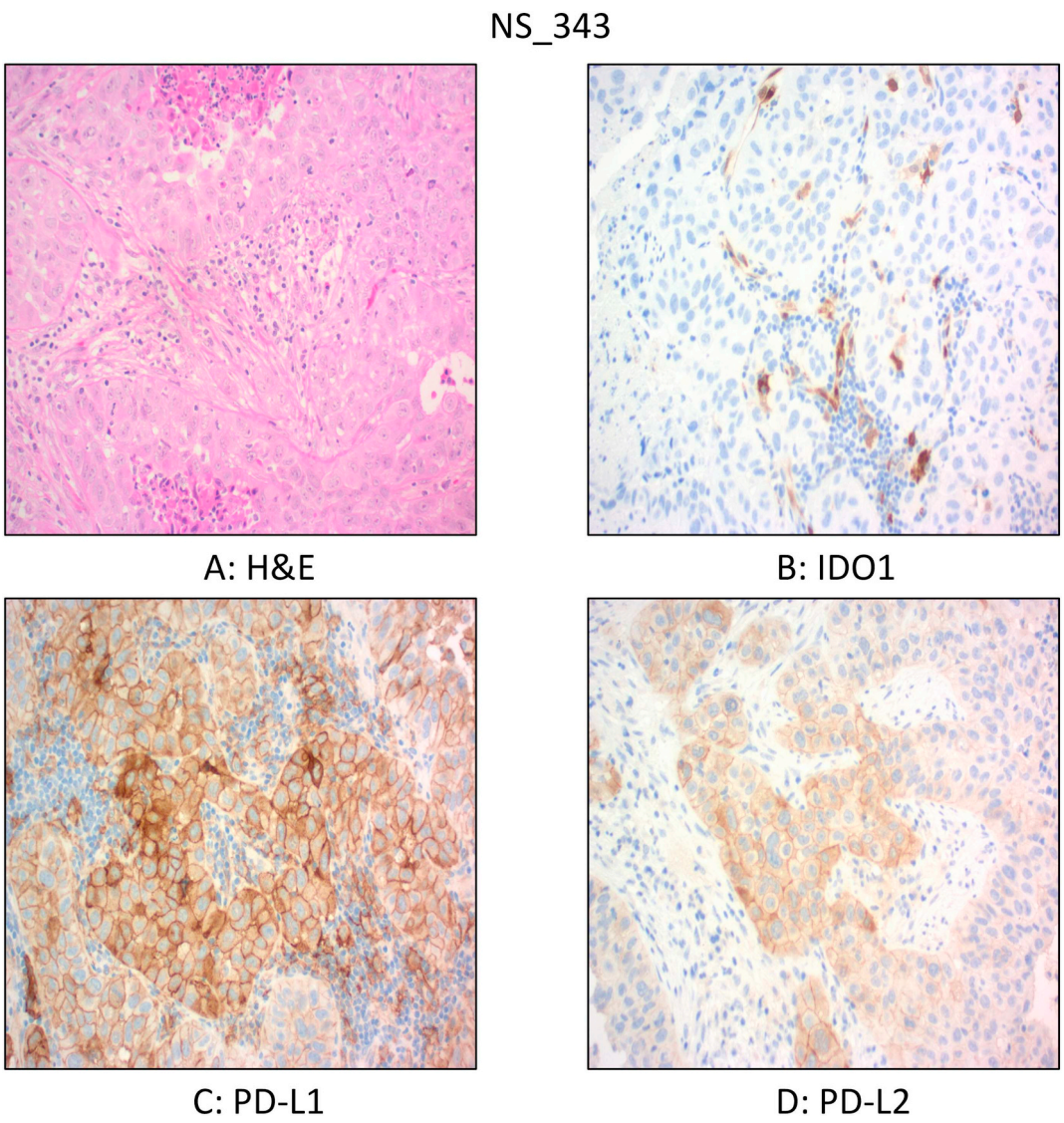

Fig. 5. Tissue sections from NS_343 were stained for H&E (Panel A), IDO1 (Panel B), PD-L1 (Panel C) and PD-L2 (Panel D) (20× magnification). Notice the positive staining of the dendritic cells and lymphocytes for IDO1. Note the positivity of the tumor (2+, focal 3+) and the surrounding lymphocytes positive for PD-L1 (PD-L2 50% of tumor at a 2+ positivity). (20× magnification). Complete Pathology scoring summary is provided in Supplementary Table S2.

NSCLC tumor (Fig. 4 and Supplementary Table S2). While tissues NS_343 and NS_350 express high levels of PD-L1, it is noteworthy that NS_343 contains a high level of CD8 cells whereas NS_350 contains low levels of CD8 cells. Despite similar PD-L1 levels in NS_343 and NS_350, the tissues are characterized by different patterns of immune-related gene expression (Figs. 2, 3 and 4).

The IHC also provides biologically relevant information regarding protein localization and distribution. For example, the transcription factor STAT3 was detected in the RNA-seq analysis, but the IHC analysis reveals that phosphorylated-STAT3 (pSTAT3) is expressed in both tumor cells and stromal cells (Supplementary Table S2). In this current IHC analysis, pSTAT3 levels do not directly correlate with the level of CD8 cells, and pSTAT3 levels vary between tissues. However, STAT3 signaling may influence tumorigenesis and the immune response (Yu et al., 2007), and therefore pSTAT3 expression data my provide insight into the nature of the anti-tumor immune response in the tumor and stroma of a given NSCLC tissue.

The variable expression of CD8 (T-cell marker) and CD163 (macrophage marker) reveals the diverse nature of the immune response in NSCLC tissues (Supplementary Table S2). The diversity of the immune response is also revealed by the observation that many of the NSCLC tissues express more than one immune inhibitory protein. For example, tissue NS_343 expresses both PD-L1 and PD-L2 (Fig. 5). Several NSCLC tissues also express the immune inhibitory proteins PD-L1 and IDO1. Tissues NS_317, NS_1342, and NS_334 express moderate (or high) levels of PDL1 and IDO1 in tumor cells (Fig. 6 and Supplementary Table S2). Interestingly, tumors NS_317 and NS_1342 are also characterized by the presence of high levels of stromal CD8+ lymphocytes, but no CD8+ lymphocytes are detected within the tumor area.

IDO1 is present in 10 tissues that also express moderate or high levels of PD-L1, and the distribution of IDO1 and PD-L1 varies within each NSCLC tissue (Supplementary Table S2). For example, PD-L1 is detected in the tumor and stroma of tissue NS_334, whereas IDO1 is solely expressed in the tumor (Fig. 6). Alternatively, PD-L1 is expressed in the tumor and surrounding stroma of tissue NS_1331, but IDO1 expression is limited to the surrounding stroma (Fig. 7). The variable expression of IDO1 and PD-L1 indicates that these that immune inhibitory proteins are expressed at unique levels within the tumor and stroma of NLSCC tissues.

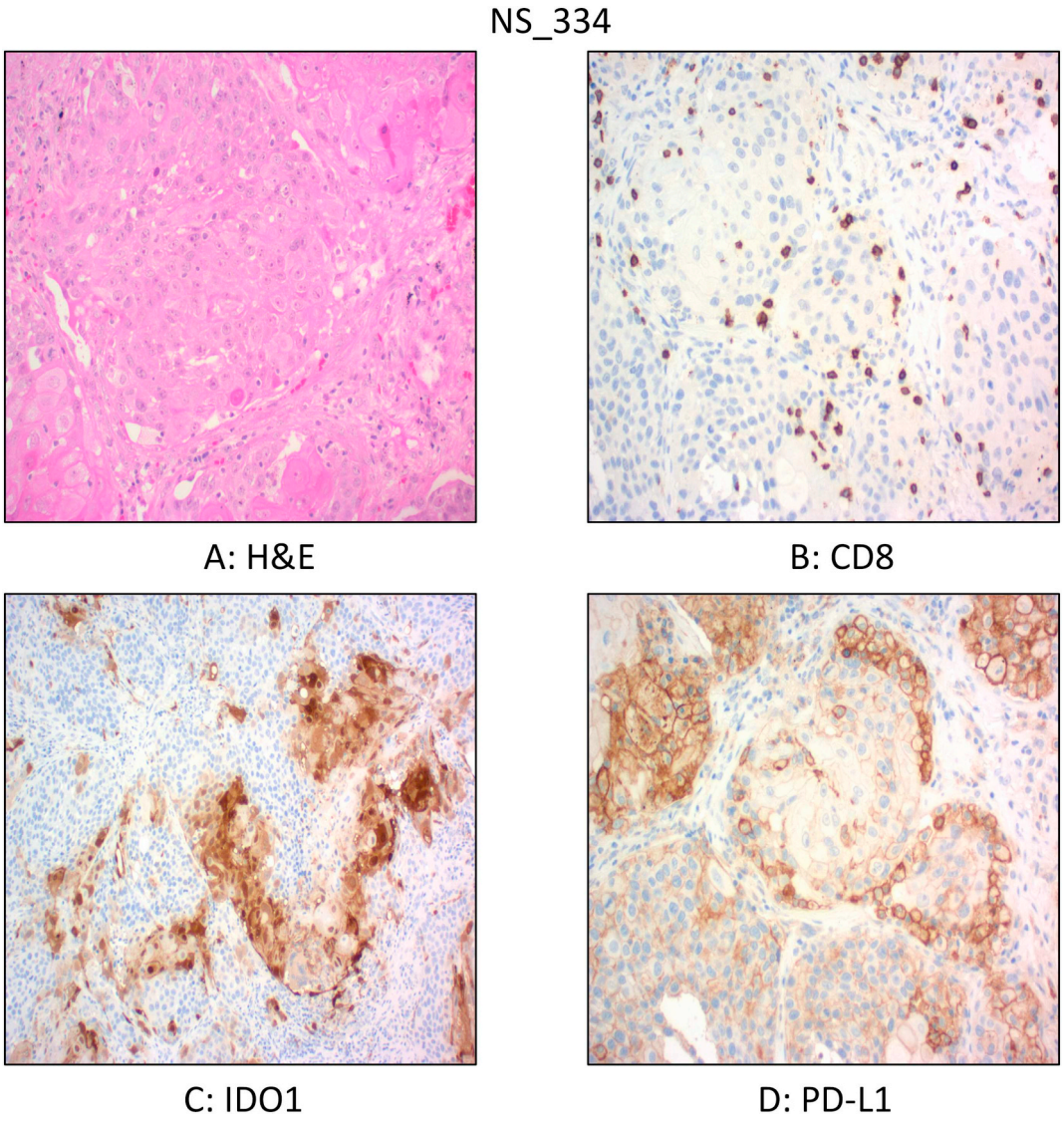

Fig. 6. Tissue sections from NS_334 were stained for H&E (Panel A), CD-8 (Few; Panel B), ID01 (Panel C) and PD-L1 (Panel D). Notice the positive staining of IDO1 tumor cells (3+), positive PD-L1 staining in the tumor (1–2+) and positive staining in the lymphocytes (2+). Complete Pathology scoring summary is provided in Supplementary Table S2.

4. Discussion

TILs are a component of the tumor microenvironment in NSCLC (Trojan et al., 2004). The TIL levels, subtype, and activation status may influence the clinical outcome (Fridman et al., 2012). In the NSCLC analysis, a T-cell marker, CD8, was used to identify T-cell levels in NSCLC tumors: low (n = 9; 40%), moderate (n = 7; 32%), or high (n = 6; 27%) (Fig. 1). CD8+ cell aggregates were more frequently observed in tumors with moderate or high CD8 levels. The CD8 aggregates may be one precursor component of tertiary lymphoid structures, which can play a role in shaping a beneficial immune response in lung cancer patients (Goc et al., 2014). In addition, the extent of CD8 infiltration may represent various states of an active anti-tumor immune response. An active tumor-immune microenvironment is important for survival and may have prognostic value (Galon et al., 2007). Moreover, an immunologically active tumor microenvironment was predictive of response to immunotherapy (Wang et al., 2002).

The RNA-seq profiling revealed significant gene expression changes among the tumors characterized by low, moderate, and high levels of CD8+ cells. The RNA-seq data revealed a putative gene signature that is associated with the levels of CD8 lymphocytes (Fig. 2). This putative CD8 gene signature contains both immune inhibitory genes and immune stimulatory genes that function in pathways related to Interferon-Gamma/STAT signaling (Tables 3 and 4). Interferon gamma may contribute to immune cell infiltration, which is an essential component of the anti-tumor immune response. Interferon/STAT signaling may also contribute to PD-L1-mediated immune suppression, PD-L1-independent immune suppression, and a multigenic resistance to an immune checkpoint blockade (Benci et al., 2016).

In addition to the putative CD8 gene signature, a subsequent analysis of the RNA-seq data aimed to characterize the expression of additional genes that may promote or inhibit an effective anti-tumor immune response in individual NSCLC tissues (Figs. 3 and 4). The NSCLC tumors possess unique combinations of genes that are associated with immune activation or immune inhibition, and the expression of immune activation or immune inhibition genes may be clinically relevant as a T-cell inflamed gene expression profile (which includes PD-L1, IDO1, STAT1, CXCL9) is associated with an improved objective response rate to anti-PD1 therapies (Ott et al., 2019).

NSCLC tissue NS_350 (CD8-low) expresses low levels of genes that function in immune activation (Fig. 3), but expresses high levels of the following immune inhibition-related genes: CD274 (PD-L1), IDO1, MIF,

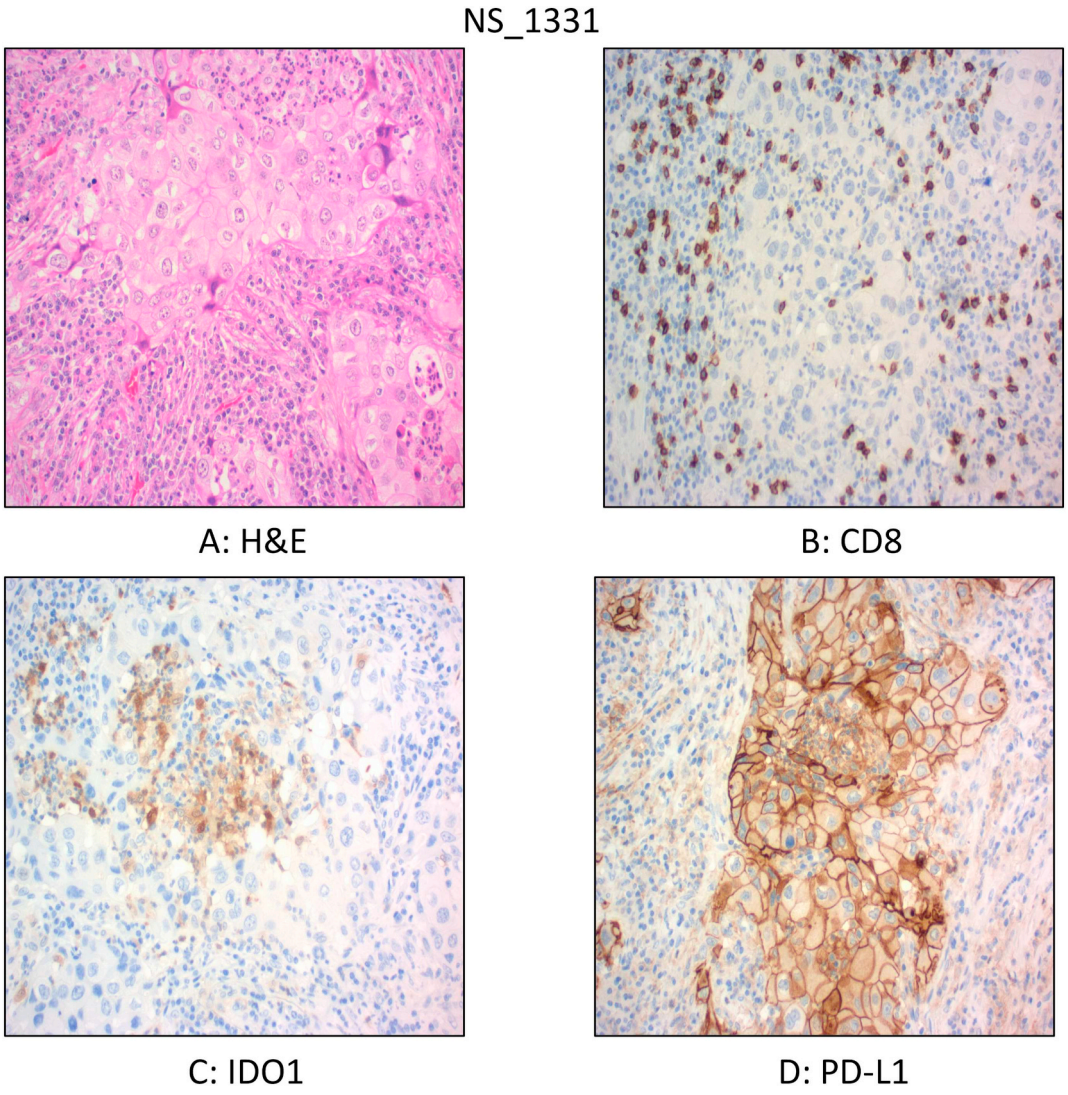

Fig. 7. Tissue sections from NS_1331 were stained for H&E (Panel A), CD8 (Moderate: Panel B), IDO1 (Panel C) and PD-L1 (Panel D) (20× magnification). Notice the positive staining of the tumor and lymphocytes surrounding the tumor for PD-L1 (3+ in the tumor). In addition, the lymphocytes are positive for IDO1. Complete Pathology scoring summary is provided in Supplementary Table S2.

CD276 (B7-H3), and LGALS3 (Galectin-3) (Fig. 4). In the current study, PD-L1 is expressed the highest level in tissue NS_350. PD-L1 is also expressed at high levels in NS_343, but NS_343 and NS_350 have different CD8 levels (NS_343: CD8 high, NS_350: CD8 low) and different gene expression profiles (Figs. 2, 3 and 4). Taken together, tissues NS_350 and NS_343 reveal that, despite high levels of PD-L1, tumor tissues may have noticeably different immune profiles. In tissue NS_350, the low levels of CD8+ cells may be due to the low expression of genes that function in immune activation (Fig. 3), which may be further disrupted by the expression of multiple genes that promote inhibitory immune signaling pathways (Fig. 4). The lack of an effective anti-tumor response may contribute to primary immunotherapy resistance (Sharma et al., 2017). Despite PD-L1 expression, a tissue may not possess enough TILs to mount a sufficient anti-tumor response following treatment targeting a single immune inhibitory checkpoint (Antonia et al., 2016). Although NS_350 expresses high levels of PD-L1, the ability to mount a clinically significant anti-tumor response may be influenced by the low level of CD8 cells in the tissue. In a clinical setting, approximately 45% PD-L1 expressing NCSLCs responded to an immune checkpoint inhibitor antibody, but the remaining PD-L1 expressing patients did not respond (Reck et al., 2016). The lack of a response, in PD-L1 expressing tumors, may also be due to the expression of additional inhibitory immune proteins (Koyama et al., 2016). A recent retrospective analysis confirmed that PD-L1 was not sufficient to predict responsiveness to PD-1/PD-L1 NSCLC immunotherapy, however, the inclusion of cytokine and immunosuppressive gene expression data (including IDO1) allowed for a more accurate prediction of NSCLC immunotherapy responders and non-responders (Brogden et al., 2018).

The CD8-high tissues NS_320, NS_326, and NS_333 co-express genes that may function in immune activation and immune inhibition. Immune-related activation genes include multiple STAT family members, TNFRSF4 (OX40), TNFRSF9 (4-1BB), TNFSF4 (OX40LG), CXCL9 (MIG), and INFG-related genes (Fig. 3 and Table S8). Tissues NS_320, NS_326, and NS_333 also express several genes that may contribute to immune inhibitory signals, such as CD276 (B7-H3), CD274 (PD-L1), IDO1, BTLA, HAVCR2 (TIM3), CD47, and genes in the CTLA4 pathway (Fig. 4 and Table S8). Taken together, the immune activation signaling may contribute to the high levels of CD8 cells, but the inhibitory immune signaling may disrupt an effective anti-tumor immune response. For example, the expression of the co-inhibitory molecule TIM3 (HAVCR2) is correlated with shorter survival in lung adenocarcinoma, and a TIM3 blockade promoted NK cell-mediated cytotoxicity (Xu et al., 2015). Tissue NS_320 also expresses the highest levels of the immune inhibitory molecule LAG3, and overall survival was previously shown

to be significantly less in lung adenocarcinoma patients with TILs that express LAG3 (He et al., 2017). Taken together, the expression of multiple immune inhibitory molecules is relevant in NSCLC as the co-expression of multiple immune inhibitory signals may contribute to immunotherapy resistance (Sharma et al., 2017; Koyama et al., 2016; Jenkins et al., 2018). It is noteworthy that 10 NSCLCs tumors co-express multiple immune inhibitory proteins (PD-L1 and IDO1; Figs. 6, 7, and Supplementary Table S2).

Overall, the RNA-seq data reveals that NSCLC tissues express a putative gene signature that is associated with CD8 cell density (low, moderate, and high CD8 levels), which may be indicative of an active anti-tumor immune response. A CD8 gene signature may have biological significance as CD8 cell infiltrate density provides information on disease prognosis and responsiveness to immunotherapy (Galon et al., 2013). In addition, the NSCLC putative CD8 gene signature contains genes that function in the INF-gamma and STAT pathways (Tables 3 and 4). The identification of INF-gamma and STAT pathway members is particularly relevant in NSCLC as INF-gamma signaling may promote an effective anti-tumor response, whereas continuous INF-gamma signaling may lead to a Jak/Stat-mediated immune escape (Benci et al., 2016; Garcia-Diaz et al., 2017; Karanikas et al., 2007).

The RNA-seq and IHC data reveal that individual NSCLC tissues may express multiple immune inhibitory molecules (Figs. 4, 5, 6, 7, and Supplementary Table S_2). The expression of multiple immune checkpoint inhibitors may explain why NSCLC tumors are initially resistant or acquire resistance to single-agent immune checkpoint therapy. IDO1 and PD-1 combination-based treatment strategies are under investigation in NSCLC (Mellemgaard et al., 2017), and this immunotherapy combination has shown promising response rates in other cancers (Fuerst, 2018; Luke et al., 2017).

Immunotherapy is also being tested in combination with treatments that target specific oncogenes within NSCLC tumors. Tyrosine kinase inhibitors (TKIs) are known to disrupt oncogenic signaling, but recent evidence suggests that TKIs may also influence the immune response (Chen et al., 2015). For example, EGFR mutations are associated with elevated levels of PD-L1 and TKI treatment may downregulate PD-L1 (Chen et al., 2015; Lin et al., 2015). Although the combination of an immune checkpoint therapy and TKIs may provide a clinical benefit, the combination may also be associated with treatment-related adverse events (Ahn et al., 2017). Improvements in molecular diagnostics may allow for the selection of patients that will benefit from therapeutic strategies that combine more than one immunotherapy treatment, or therapeutic strategies that combine targeted therapy with immunotherapy.

Recent testing strategies, including tumor mutational burden (TMB), microsatellite instability (MSI), PD-L1 IHC, and gene expression assays, may have value in predicting responsiveness to immune checkpoint therapy (Ott et al., 2019; Voong et al., 2017; Ribas et al., 2015). However, TMB, MSI, PD-L1, and gene expression assays may provide more value when they are synergistically applied to individual tumors. Preliminary evidence suggests that a composite biomarker, consisting of PD-L1 IHC and INF-gamma mRNA testing, is associated with response to immune checkpoint therapy in NSCLC (Voong et al., 2017; Higgs et al., 2016). Although our data provides insight into potential NSCLC biomarkers, our study is limited to the small sample size and lack of clinical outcome data. Therefore, our results need to be examined within the context of a larger NSCLC cohort with clinical outcomes. A larger cohort may yield more definitive conclusions regarding the use of the current data for the selection of standalone or composite biomarkers for NSCLC immunotherapies.

Appendix A. Supplementary data

Supplementary data to this article can be found online at https://doi.org/10.1016/j.yexmp.2019.04.004.

References

ACS, 2018. The Cancer Atlas-Explore The Burden-Lung Cancer. [cited 2018 2018]; Available from: http://canceratlas.cancer.org/the-burden/lung-cancer.

Ahn, M.J., et al., 2017. EGFR TKI combination with immunotherapy in non-small cell lung cancer. Expert Opin. Drug Saf. 16 (4), 465–469.

Alomari, A.K., et al., 2016. Possible interaction of anti-PD-1 therapy with the effects of radiosurgery on brain metastases. Cancer Immunol. Res. 4 (6), 481–487.

Antonia, S.J., Vansteenkiste, J.F., Moon, E., 2016. Immunotherapy: beyond anti-PD-1 and anti-PD-L1 therapies. Am. Soc. Clin. Oncol. Educ. Book 35, e450–e458.

Baxi, S., et al., 2018. Immune-related adverse events for anti-PD-1 and anti-PD-L1 drugs: systematic review and meta-analysis. BMJ 360, k793.

Benci, J.L., et al., 2016. Tumor interferon signaling regulates a multigenic resistance program to immune checkpoint blockade. Cell 167 (6), 1540–1554 (e12).

Brogden, K.A., et al., 2018. Genomics of NSCLC patients both affirm PD-L1 expression and predict their clinical responses to anti-PD-1 immunotherapy. BMC Cancer 18 (1), 225.

Champiat, S., et al., 2017. Hyperprogressive disease is a new pattern of progression in cancer patients treated by anti-PD-1/PD-L1. Clin. Cancer Res. 23 (8), 1920–1928.

Chang, L., et al., 2018 Feb. Microsatellite instability: a predictive biomarker for cancer immunotherapy. Appl. Immunohistochem. Mol. Morphol. 26 (2), e15–e21. https://www.pubfacts.com/detail/28877075/Microsatellite-Instability-A-Predictive-Biomarker-for-Cancer-Immunotherapy.

Chen, Z., et al., 2014. Non-small-cell lung cancers: a heterogeneous set of diseases. Nat. Rev. Cancer 14 (8), 535–546.

Chen, N., et al., 2015. Upregulation of PD-L1 by EGFR activation mediates the immune escape in EGFR-driven NSCLC: implication for optional immune targeted therapy for NSCLC patients with EGFR mutation. J. Thorac. Oncol. 10 (6), 910–923.

Dang, T.O., et al., 2016. Pembrolizumab for the treatment of PD-L1 positive advanced or metastatic non-small cell lung cancer. Expert. Rev. Anticancer. Ther. 16 (1), 13–20.

De Simone, M., et al., 2016. Transcriptional landscape of human tissue lymphocytes unveils uniqueness of tumor-infiltrating T regulatory cells. Immunity 45 (5), 1135–1147.

Dela Cruz, C.S., Tanoue, L.T., Matthay, R.A., 2011. Lung cancer: epidemiology, etiology, and prevention. Clin. Chest Med. 32 (4), 605–644.

Ettinger, D.S., et al., 2017. Non-small cell lung cancer, version 5.2017, NCCN clinical practice guidelines in oncology. J. Natl. Compr. Cancer Netw. 15 (4), 504–535.

FDA, 2017. Hematology/Oncology (Cancer) Approvals & Safety Notifications. Approved Drug 2017 01/26/2018 [cited 2017; Available from: https://www.fda.gov/Drugs/InformationOnDrugs/Approved Drugs/ucm279174.htm.

Fridman, W.H., et al., 2012. The immune contexture in human tumours: impact on clinical outcome. Nat. Rev. Cancer 12 (4), 298–306.

Fuerst, M.L., 2018. Nivolumab Plus IDO Inhibitor Promising in Pretreated Bladder and Cervical Cancers - Strong Rationale for Further Studies Targeting these Two Immune Checkpoint Pathways. MEDPAGETODAY (ASCO).

Galon, J., Fridman, W.H., Pages, F., 2007. The adaptive immunologic microenvironment in colorectal cancer: a novel perspective. Cancer Res. 67 (5), 1883–1886.

Galon, J., et al., 2013. The continuum of cancer immunosurveillance: prognostic, predictive, and mechanistic signatures. Immunity 39 (1), 11–26.

Garcia-Diaz, A., et al., 2017. Interferon receptor signaling pathways regulating PD-L1 and PD-L2 expression. Cell Rep. 19 (6), 1189–1201.

Gettinger, S., et al., 2016. Nivolumab monotherapy for first-line treatment of advanced non-small-cell lung cancer. J. Clin. Oncol. 34 (25), 2980–2987.

Goc, J., et al., 2014. Tertiary lymphoid structures in human lung cancers, a new driver of antitumor immune responses. Oncoimmunology 3, e28976.

Hamm, C.A., et al., 2016. Genomic and immunological tumor profiling identifies targetable pathways and extensive CD8+/PDL1+ immune infiltration in inflammatory breast cancer tumors. Mol. Cancer Ther. 15 (7), 1746–1756.

He, Y., et al., 2017. LAG-3 protein expression in non-small cell lung cancer and its relationship with PD-1/PD-L1 and tumor-infiltrating lymphocytes. J. Thorac. Oncol. 12 (5), 814–823.

Higgs, B.W., et al., 2016. Relationship of Baseline Tumoral IFNγ mRNA and PD-L1 Protein Expression to Overall Survival in Durvalumab-Treated NSCLC Patients. American Society of Clinical Oncology.

J, B., et al., 2017. Five-year follow-up from the CA209-003 study of nivolumab in previously treated advanced non-small cell lung cancer (NSCLC): Clinical characteristics of long-term survivors. In: American Association for Cancer Research. AACR, Washington, DC.

Jenkins, R.W., Barbie, D.A., Flaherty, K.T., 2018. Mechanisms of resistance to immune checkpoint inhibitors. Br. J. Cancer 118 (1), 9–16.

Kang, P., S., et al., 2017. Pembrolizumab KEYNOTE-001: An adaptive study leading to accelerated approval for two indications and a companion diagnostic. 28. pp. 1388–1398.

Karanikas, V., et al., 2007. Indoleamine 2, 3-dioxygenase (IDO) expression in lung cancer. Cancer Biol. Ther. 6 (8), 1258–1262.

Kouo, T., et al., 2015. Galectin-3 shapes antitumor immune responses by suppressing CD8+ T cells via LAG-3 and inhibiting expansion of plasmacytoid dendritic cells. Cancer Immunol. Res. 3 (4), 412–423.

Kowanetz, M., et al., OA20.01 tumor mutation burden (TMB) is associated with improved efficacy of atezolizumab in 1L and 2L+ NSCLC patients. J. Thorac. Oncol. 12(1): p. S321-S322.

Koyama, S., et al., 2016. Adaptive resistance to therapeutic PD-1 blockade is associated with upregulation of alternative immune checkpoints. Nat. Commun. 7, 10501.

Lin, K., et al., 2015. EGFR-TKI down-regulates PD-L1 in EGFR mutant NSCLC through inhibiting NF-kappaB. Biochem. Biophys. Res. Commun. 463 (1–2), 95–101.

Liu, X., et al., 2017. Is CD47 an innate immune checkpoint for tumor evasion? J. Hematol. Oncol. 10 (1), 12.
Luke, J.L.G.K., Pachynski, R.K., Desai, J., Moreno, V., Tabernero, J.M., Gomez-Roca, C.A., Chu, Q., Basciano, P., Phillips, P., Liu, Z., Siu, L.L., 2018. Preliminary antitumor and immunomodulatory activity of BMS-986205, an optimized indoleamine 2,3-dioxygenase 1 (IDO1) inhibitor, in combination with nivolumab in patients with advanced cancers. In: Annual Meeting and Pre-Conference Programs of the Society for Immunotherapy of Cancer (SITC 2017). National Harbor MD.
Malhotra, J., Jabbour, S.K., Aisner, J., 2017. Current state of immunotherapy for non-small cell lung cancer. Transl. Lung Cancer Res. 6 (2), 196–211.
Mellemgaard, A., et al., 2017. Combination immunotherapy with IDO vaccine and PD-1 inhibitors in advanced NSCLC. J. Clin. Oncol. 35 (15_suppl), TPS2610.
Munn, D.H., Mellor, A.L., 2007. Indoleamine 2, 3-dioxygenase and tumor-induced tolerance. J. Clin. Invest. 117 (5), 1147–1154.
Oelkrug, C., Ramage, J.M., 2014. Enhancement of T cell recruitment and infiltration into tumours. Clin. Exp. Immunol. 178 (1), 1–8.
Ott, P.A., et al., 2019. T-cell-inflamed gene-expression profile, programmed death ligand 1 expression, and tumor mutational burden predict efficacy in patients treated with pembrolizumab across 20 cancers: KEYNOTE-028. J. Clin. Oncol. 37 (4), 318–327.
Pardoll, D.M., 2012. The blockade of immune checkpoints in cancer immunotherapy. Nat. Rev. Cancer 12 (4), 252–264.
Ramalingam, S., et al., 2016. P 2.39: long-term OS for patients with advanced NSCLC enrolled in the KEYNOTE-001 study of pembrolizumab: track: immunotherapy. J. Thorac. Oncol. 11 (10S), S241–S242.
Reck, M., et al., 2016. Pembrolizumab versus chemotherapy for PD-L1-positive non-small-cell lung cancer. N. Engl. J. Med. 375 (19), 1823–1833.
Ribas, A., et al., 2015. Association of Response to Programmed Death Receptor 1 (PD-1) Blockade With Pembrolizumab (MK-3475) With an Interferon-Inflammatory Immune Gene Signature[Abstract]. 33.
Sharma, P., et al., 2017. Primary, adaptive, and acquired resistance to cancer immunotherapy. Cell 168 (4), 707–723.
Somasundaram, A., Burns, T.F., 2017. The next generation of immunotherapy: keeping lung cancer in check. J. Hematol. Oncol. 10 (1), 87.
Subramanian, A., et al., 2005. Gene set enrichment analysis: a knowledge-based approach for interpreting genome-wide expression profiles. Proc. Natl. Acad. Sci. U. S. A. 102 (43), 15545–15550.
Trojan, A., et al., 2004. Immune activation status of CD8+ T cells infiltrating non-small cell lung cancer. Lung Cancer 44 (2), 143–147.
Voong, K.R., et al., 2017. Beyond PD-L1 testing-emerging biomarkers for immunotherapy in non-small cell lung cancer. Ann. Transl. Med. 5 (18), 376.
Wang, E., et al., 2002. Prospective molecular profiling of melanoma metastases suggests classifiers of immune responsiveness. Cancer Res. 62 (13), 3581–3586.
Wherry, E.J., Kurachi, M., 2015. Molecular and cellular insights into T cell exhaustion. Nat. Rev. Immunol. 15 (8), 486–499.
Workman, C.J., Vignali, D.A., 2003. The CD4-related molecule, LAG-3 (CD223), regulates the expansion of activated T cells. Eur. J. Immunol. 33 (4), 970–979.
Workman, C.J., et al., 2004. Lymphocyte activation gene-3 (CD223) regulates the size of the expanding T cell population following antigen activation in vivo. J. Immunol. 172 (9), 5450–5455.
Xu, L., et al., 2015. Increased Tim-3 expression in peripheral NK cells predicts a poorer prognosis and Tim-3 blockade improves NK cell-mediated cytotoxicity in human lung adenocarcinoma. Int. Immunopharmacol. 29 (2), 635–641.
Yu, H., Kortylewski, M., Pardoll, D., 2007. Crosstalk between cancer and immune cells: role of STAT3 in the tumour microenvironment. Nat. Rev. Immunol. 7 (1), 41–51.